doi: 10.82124/CEAS-GNC-2026-040 CEAS-GNC-2026-040

Evolution of Robust Navigation Towards the Aerial Environment

Santiago García Samartín Homeland Security & Defense GMV, Madrid, Spain. sags@gmv.com

Javier Ferrero Micó Homeland Security & Defense GMV, Madrid, Spain. jffm@gmv.com

Mikel Loinaz Anton Homeland Security & Defense GMV, Madrid, Spain. mikel.loinaz.anton@gmv.com

Carmen María Haro Montero INDRA Group, Madrid, Spain. cmmonteroh@indra.es

Joao Vieira Caetano European Defence Agency, Single European Sky Unit, Brussels, Belgium. Joao.CAETANO@eda.europa.eu

ABSTRACT

Unmanned Aircraft Systems (UAS) flights rely on the ability to determine their position with high accuracy and continuity, even in degraded environments. Traditional localisation approaches combine data from Global Navigation Satellite Systems (GNSS) and Inertial Measurement Units (IMUs), which together provide reliable navigation under nominal conditions. However, the increasing sophistication of jamming and spoofing threats has exposed the dependence of these systems on external signals, creating a demand for alternative methods that can ensure precise navigation when GNSS data becomes unreliable or unavailable. To address this challenge, this work explores the integration of classical navigation sensors with artificial intelligence techniques to enhance precision in navigation, as well as robustness in complex environments. The proposed framework combines IMU and GNSS information with visual data processed through deep learning algorithms for odometry estimation and map correlation. All measurements are subsequently fused within an Extended Kalman Filter (EKF), which provides an optimal estimation of the vehicle state and dynamically balances sensor contributions according to their estimated reliability. The resulting system enables UAS to adaptively select the most accurate and stable source of navigation data depending on mission context, terrain visibility, and environmental conditions. Beyond the technical contribution, this approach aims to reduce operational dependency on external infrastructure while improving safety in autonomous flight missions. The proposed architecture is systematically evaluated by comparing different sensor configurations, using the classical GNSS+IMU solution as a reference baseline. This controlled assessment allows the contribution and limitations of visual aiding to be clearly quantified relative to standard navigation performance. The results demonstrate the feasibility of deploying visual-aided navigation as a resilient complementary component within small UAS Positioning, Navigation, and Timing (PNT) architectures, while identifying robustness to visual outliers as a key avenue for further performance enhancement.

Keywords: UAS, Deep learning, visual navigation, self-localization, GNSS denied environments

Except where otherwise noted, content of this paper is licensed under a Creative Commons Attribution 4.0 International License.

The reproduction and distribution with attribution of the entire paper or of individual pages, in electronic or printed form, including any material under non-CC-BY 4.0 licenses is hereby granted by the authors and respective copyright owners.

1 Introduction

Precise Positioning, Navigation, and Timing (PNT) for aerial vehicles constitutes a key enabler in current operational frameworks, where autonomous systems have demonstrated high performance across diverse tactical scenarios. At present, Global Navigation Satellite Systems (GNSS) remain the primary reference for high-accuracy localisation and time synchronisation, serving not only as the basis for multi-sensor navigation fusion but also as a core input to aircraft subsystems such as communications, which underpin emerging operational concepts including swarming and manned–unmanned teaming.

However, as these applications grow increasingly dependent on GNSS, their inherent vulnerabilities become more pronounced. Electronic warfare threats such as jamming, which saturate the receiver with high-power interference, and spoofing, which injects counterfeit satellite-like signals to mislead the navigation solution, represent major risks to system integrity. Beyond adversarial attacks, GNSS also exhibits performance degradation in constrained environments such as urban canyons, dense foliage, or indoor settings, where multipath propagation and signal attenuation lead to reduced availability and accuracy.

Several strategies have been explored to enable navigation when GNSS is unavailable or degraded. Traditional approaches either limit interference using military receivers such as GPS M-code and PRS or Controlled Reception Pattern Antennas (CRPA), or to rely on Inertial Measurement Units (IMUs) combined with auxiliary sensors, such as magnetometers or dead-reckoning techniques Ref. [1]. While the former enhance resilience against jamming and spoofing, the latter are affected by drift, since navigation accuracy depends largely on the quality of the Inertial Navigation System (INS).

To address these limitations, recent research has focused on improving INS performance through advanced estimation and sensor modelling techniques. One research direction incorporates artificial intelligence into the IMU mechanisation process, leading to more robust and adaptive estimation of attitude and position Ref. [2]. Neural network-based calibration methods have also been proposed to correct systematic IMU errors, thereby reducing long-term drift accumulation Ref. [3].

In parallel, significant progress has been made in the development of quantum-based inertial sensors, including miniaturised quantum systems for IMUs Ref. [4, 5] and cold-atom interferometry using rubidium (Rb) atoms Refs. [6, 7]. These technologies offer the potential for drift-free navigation by providing highly precise measurements of acceleration and rotation. However, despite promising experimental results, their Technology Readiness Level (TRL) remains limited for operational aerial applications.

Magnetometers can also improve attitude estimation or support Magnetic Anomaly Navigation (MagNav). In this approach, navigation is performed by comparing in-situ magnetic readings with reference anomaly maps of the Earth's crustal magnetic field Refs. [8, 9]. More recently, the integration of quantum magnetometers has been investigated to enhance navigation accuracy, as these devices enable precise magnetic field measurements Refs. [10–12]

Another research line focuses on vision-based navigation, which is currently among the most mature alternatives for GNSS-denied operation. Cameras are frequently integrated with other sensors to mitigate INS drift. They can be employed either for visual odometry Refs. [13, 14] or for map-matching techniques Ref. [15–20]. In the first case, navigation relies on tracking features between consecutive images, whereas map matching aligns camera images with pre-existing georeferenced maps of the area. These approaches are effective in environments where distinctive features can be extracted and under favorable visibility conditions, and they already exhibit a high TRL for practical applications.

Building on these advances, this work introduces an integrated navigation system designed for UAS operations in degraded or denied GNSS environments. The proposed architecture combines complementary sensors, including an IMU, electro-optical and infrared cameras, and a GNSS receiver with anti-spoofing capabilities, all integrated within a unified Kalman filter framework that ensures continuous and reliable

Except where otherwise noted, content of this paper is licensed under a Creative Commons Attribution 4.0 International License.

The reproduction and distribution with attribution of the entire paper or of individual pages, in electronic or printed form, including any material under non-CC-BY 4.0 licenses is hereby granted by the authors and respective copyright owners.

state estimation under diverse conditions. The development follows a structured validation process that includes simulations and hardware-in-the-loop testing. The current stage of the project corresponds to the Hardware-in-the-Loop (HIL) demonstration, which constitutes the final step before integration into the UAS platform and enables functional verification prior to flight deployment.

2 Related work

Commercial navigation systems with high TRL levels are already available on the market. Early UAS navigation relied on the integration of GNSS and IMU data to obtain the navigation solution, an approach highly dependent on IMU performance when GNSS signals are degraded or unavailable. High-grade IMUs developed by leading manufacturers Refs. [21–24], usually based on ring-laser or fiber-optic gyroscopes and low-drift accelerometers, provide very stable inertial measurements and accurate dead-reckoning under GNSS-denied conditions. However, these sensors achieve such precision at the expense of high cost, considerable weight, and larger dimensions, which makes the overall navigation solution expensive and unsuitable for integration in many UAS platforms.

Most of these developments have originated in the United States, although Europe has also made notable advances, with emerging solutions offering competitive performance and reduced size, weight, and power consumption. Representative examples include the UMIX series from iXblue and the STIM318 from Sensonor Refs. [25, 26], which employ fibre-optic and MEMS technologies, respectively, to deliver tactical-grade performance with drift rates below one degree per hour. However, these IMUs still require complementary sensors to maintain reliable navigation in GNSS-denied environments.

In this context, emerging solutions have explored the use of other sensors to combine with inertial measurements whose main goal is to contain the solution's overall drift. State-of-the-art approaches frequently integrate LiDAR, cameras, GNSS, and even magnetic field sensing to improve pose estimation and robustness in challenging or GNSS-denied environments. For example, LOAM (LiDAR Odometry and Mapping) Ref. [27] tightly couples LiDAR and IMU data for precise real-time localisation, while VINS-Mono Ref. [28] fuses monocular vision and IMU readings to address drift. Inertial Labs has proposed the integration of cameras with the IMU Ref. [29]. This visual–inertial navigation system (VINS) combines inertial data with visual cues extracted from sequential images. The IMU provides high-frequency motion updates that stabilize the short-term solution, while the camera constrains the drift through feature tracking and scene reconstruction. Similarly, Ref. [30] explores the fusion of these sensors using artificial intelligence techniques, leveraging neural networks to model sensor errors and adaptively weight their contributions.

LIO-SAM (LiDAR-Inertial Odometry via Smoothing and Mapping) Ref. [31] further exploits factor graph optimization for enhanced drift mitigation. Additionally, algorithms such as ROVIO (Robust Visual-Inertial Odometry) Ref. [32] and A-LOAM Ref. [33] leverage visual and inertial cues, and recent research has also incorporated magnetometer data to augment orientation accuracy. Approaches like magneto-inertial fusion, cf. Ref. [34] and Ref. [35], exploit magnetic anomalies—regions with distinctive geomagnetic signatures—to provide additional constraints for orientation, reduce long-term drift, and overcome limitations of inertial-only systems in environments with unique magnetic field distributions.

The fact that the majority of the mature solutions were developed in the United States underscores the need for Europe to design navigation systems capable of matching their performance, if it aims to remain a global technological power and ensure the security of its borders. The solution outlined in this work seeks to develop a navigator that integrates classical sensors such as IMUs and GNSS with cameras to achieve robust navigation under all possible operational scenarios. Furthermore, its modular architecture allows the incorporation of additional sensors, such as magnetometers, to continuously enhance and adapt the system to emerging requirements and constraints.

Except where otherwise noted, content of this paper is licensed under a Creative Commons Attribution 4.0 International License.

The reproduction and distribution with attribution of the entire paper or of individual pages, in electronic or printed form, including any material under non-CC-BY 4.0 licenses is hereby granted by the authors and respective copyright owners.

3 Validation and Verification Environment

To introduce these new approaches into the navigation system and evaluate their performance, it is key to do it in a closed loop so that the whole system evolves along the navigation solution.

To do so, an ad-hoc hardware-in-the-loop environment has been developed, where a sensor Sim, cf. Fig. 1, provides the different sensors' raw data, which shall then be processed in runtime by the different algorithms. The PNT system is composed of two different cores: the NAV core and the ALTERNATIVE core. While the NAV core holds the main Navigation capabilities and algorithms, which are already validated through GMV's different product families: SENDA for maritime domain, ISNAV for land solutions and NERVA for aerial navigation systems, the ALTERNATIVE core is populated with all sorts of new algorithms which have been assessed to be of interest.

Finally, the navigation solution is produced in each step, and it is sent to the Flight Dynamics Simulator, which will then provide the new input for the next step of sensors' raw data.

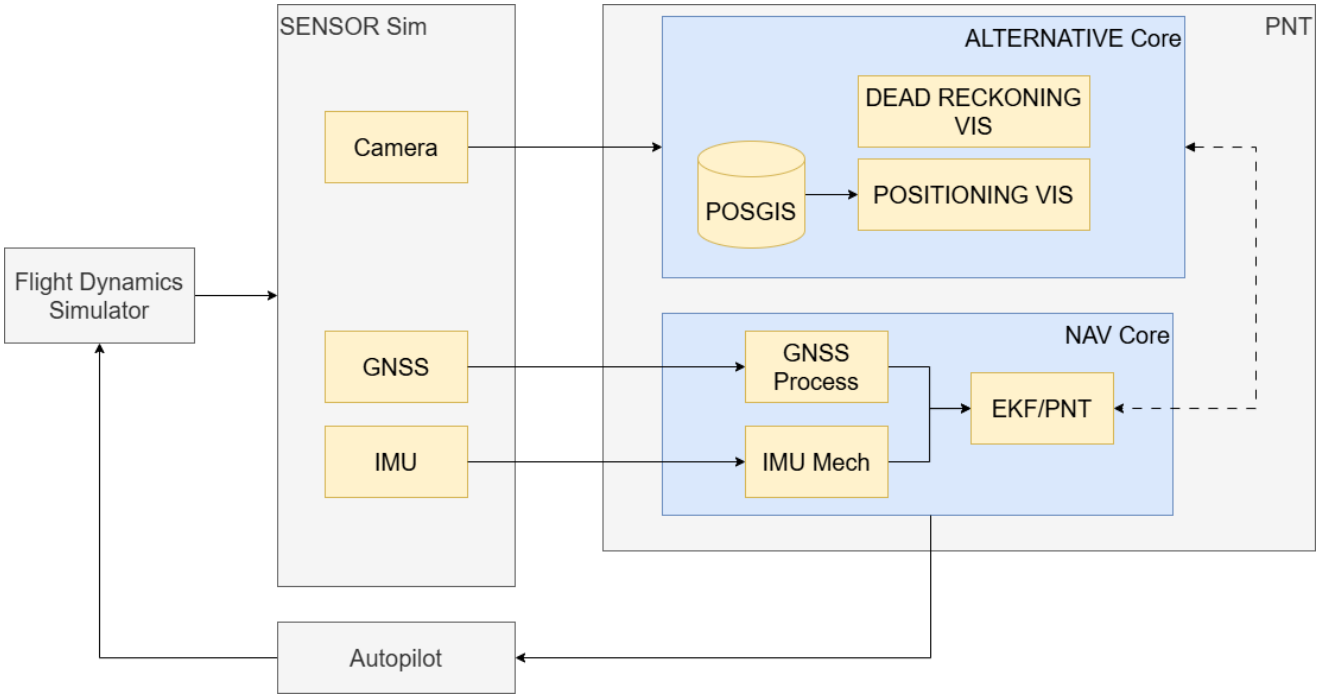

Fig. 1 System architecture

In the following sections, further detail on the composition of both NAV Core and ALTERNATIVE Core is given.

3.1 NAV Core

The NAV Core constitutes the execution environment for all navigation functions, operating on a Linux system deployed over a certifiable CPU. This architecture enables the integration of advanced capabilities alongside mature navigation components, thereby supporting both rigorous verification and efficient transition to operational systems.

Within this framework, GNSS and IMU measurements are processed as primary inputs. All data streams are synchronized using the PPS signal, ensuring temporal consistency and enabling real-time propagation of the navigation solution.

Based on these synchronized inputs, the system implements a multi-sensor fusion strategy to obtain a robust navigation estimate. Inertial measurements are processed through IMU mechanization, providing continuous estimates of attitude, velocity, and position. When available, GNSS observables supply

Except where otherwise noted, content of this paper is licensed under a Creative Commons Attribution 4.0 International License.

The reproduction and distribution with attribution of the entire paper or of individual pages, in electronic or printed form, including any material under non-CC-BY 4.0 licenses is hereby granted by the authors and respective copyright owners.

absolute positioning and timing information. In addition, visual navigation outputs are incorporated. All measurements are fused within an Extended Kalman Filter (EKF), which exploits the complementary characteristics of each sensor to mitigate error growth and ensure a consistent state estimate.

Mechanisation process enables continuous state propagation between measurement updates. However, in the absence of external corrections, sensor noise and biases lead to drift. This limitation is addressed through EKF updates, which incorporate external observations—including GNSS and visual navigation—to bound error growth. Consequently, the INS serves both as a short-term autonomous navigation solution and as the predictive model underpinning the estimation framework.

The GNSS module provides the primary source of absolute positioning with high accuracy and availability by leveraging multi-constellation (GPS, GLONASS, Galileo) and multi-frequency operation. It integrates SBAS corrections and internal integrity monitoring algorithms to enhance robustness. Spoofing detection mechanisms are also included to identify potential interference. The architecture supports dual-receiver configurations, enabling either redundant civil operation or hybrid civil–military setups. Depending on the configuration, navigation solutions may be computed jointly or separated by constellation or signal type.

The EKF constitutes the core estimation engine of the proposed navigation architecture, enabling the consistent fusion of heterogeneous sensor data within a unified probabilistic framework. By combining inertial, GNSS, and visual measurements, the filter provides a single, coherent estimate of the vehicle state, which is essential for reliable operation in complex and degraded environments.

In this context, the EKF plays a central role in managing sensor complementarities and limitations. Inertial measurements ensure high-rate continuity but are subject to drift, GNSS provides absolute positioning but may be degraded or denied, and visual navigation offers relative corrections that depend on environmental conditions. The EKF integrates these sources by explicitly modelling their uncertainties, allowing each sensor to contribute according to its estimated reliability.

This uncertainty-driven fusion mechanism is particularly critical for robustness. Through the propagation of the state covariance and the evaluation of measurement innovations, the EKF continuously assesses the consistency of incoming data with respect to the predicted state. As a result, degraded or inconsistent measurements (such as those affected by GNSS interference or visual outliers) can be down-weighted or rejected, preventing them from corrupting the navigation solution.

Furthermore, the EKF naturally supports asynchronous and multi-rate sensor integration, which is required in practical systems where IMU, GNSS, and vision operate at different frequencies and latencies. This capability enables seamless incorporation of visual navigation into the estimation process without requiring structural modifications to the overall architecture.

The formulation adopted in this work follows the standard EKF approach for nonlinear state estimation, based on first-order linearization of the system dynamics and measurement models, as widely established in the literature Refs. [1, 36, 37]. This centralised fusion approach is fundamental to the proposed architecture, as it enables adaptive sensor utilisation and ensures navigation continuity under varying operational conditions.

3.2 ALTERNATIVE Core

The ALTERNATIVE Core provides a flexible execution environment for the development and validation of vision-based navigation capabilities, operating on a Linux-based system over a GPU platform. Unlike conventional navigation architectures, which are typically constrained to fixed processing chains, this framework enables rapid integration, deployment, and benchmarking of heterogeneous algorithms through containerised services (Docker/Kubernetes). This capability is essential to iteratively evaluate different visual navigation strategies within a closed-loop system, maintaining consistency with the overall navigation architecture while allowing modular upgrades.

Except where otherwise noted, content of this paper is licensed under a Creative Commons Attribution 4.0 International License.

The reproduction and distribution with attribution of the entire paper or of individual pages, in electronic or printed form, including any material under non-CC-BY 4.0 licenses is hereby granted by the authors and respective copyright owners.

The primary objective of the ALTERNATIVE Core is to augment the navigation solution with vision-based estimates that improve robustness in GNSS-degraded or denied environments. To this end, the module processes camera imagery together with associated metadata and the latest EKF state, producing position estimates that are reinjected into the global fusion framework. This tight integration with the EKF differentiates the proposed approach from loosely coupled or standalone vision-based solutions, as it ensures statistical consistency and real-time adaptability within the overall navigation system. To do so, it combines two complementary strategies: visual odometry, which provides short-term relative motion estimation, and map correlation, which enables absolute position updates. This dual approach addresses a key limitation of standalone methods, where odometry alone suffers from drift and map-based approaches alone may be intermittent or computationally expensive. By jointly exploiting both mechanisms within the same framework, the system achieves both continuity and global consistency.

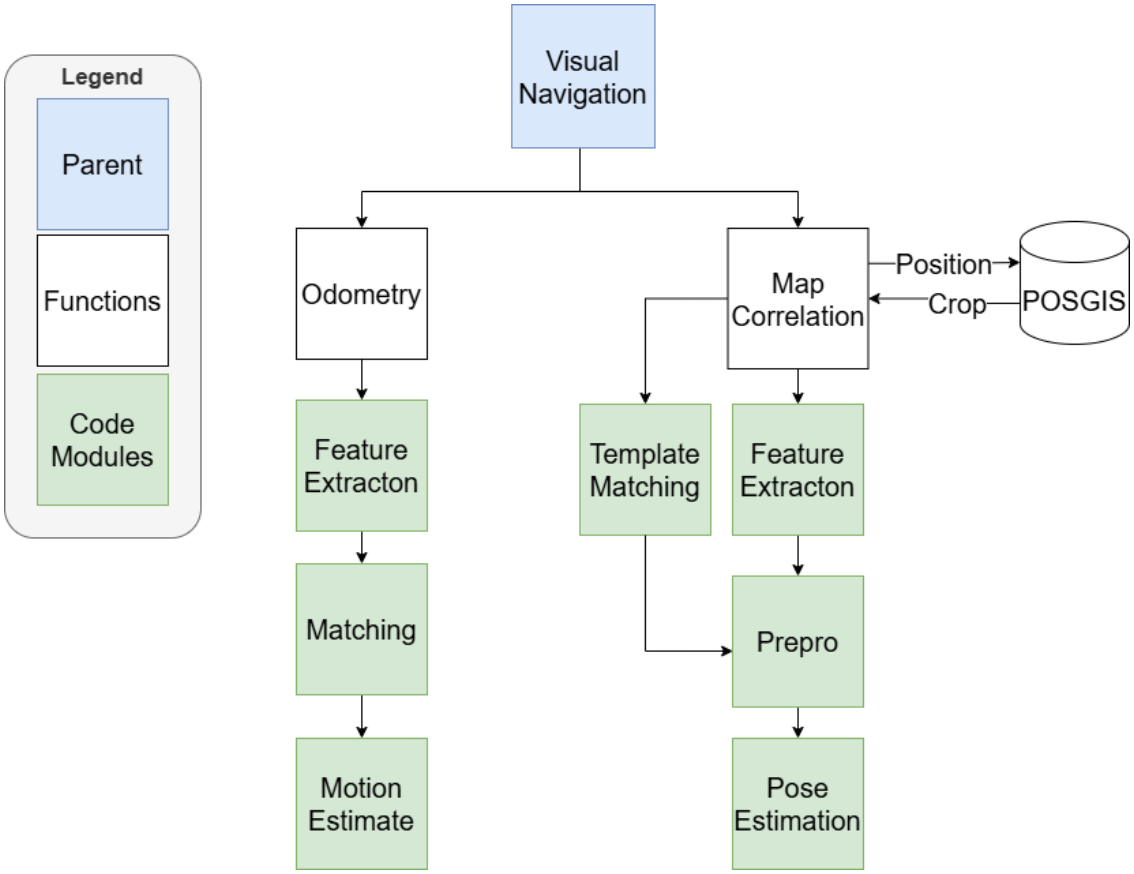

Fig. 2 Visual Navigation Module High Level Architecture

Focusing on the visual odometry module, it provides high-rate relative motion estimates derived from sequential image analysis. By tracking salient features across consecutive frames and estimating their geometric transformation, the module enables continuous trajectory propagation independently of external signals. When integrated within the EKF, these measurements provide complementary motion constraints to the inertial solution: while the INS exhibits drift due to bias integration, visual odometry introduces independent relative estimates that help bound error growth. This interaction results in improved short-term accuracy and enhanced trajectory stability compared to standalone inertial or vision-based approaches.

In contrast, the map correlation module provides absolute position updates by matching onboard imagery with georeferenced orthophotos. This capability is particularly relevant in GNSS-denied scenarios, where absolute positioning must be recovered without reliance on external signals. By leveraging prior map information, the module effectively re-anchors the navigation solution, reducing long-term drift and improving global accuracy. The use of the EKF state as prior information further constrains the search

Except where otherwise noted, content of this paper is licensed under a Creative Commons Attribution 4.0 International License.

The reproduction and distribution with attribution of the entire paper or of individual pages, in electronic or printed form, including any material under non-CC-BY 4.0 licenses is hereby granted by the authors and respective copyright owners.

space, improving both robustness and computational efficiency compared to standalone image-to-map matching approaches.

The combination of relative (odometry) and absolute (map correlation) visual measurements within a unified fusion framework constitutes a key differentiator of the proposed approach. Rather than relying on a single modality, the system dynamically exploits the complementary properties of each method, enabling adaptive performance across varying environmental conditions. This is particularly relevant in real-world operations, where scene texture, illumination, and map availability may vary throughout the mission.

In contrast to many state-of-the-art vision-based navigation systems based on Simultaneous Localization and Mapping (SLAM), the proposed approach does not rely on online map generation. SLAM-based methods typically require persistent scene overlap and are therefore best suited for low-altitude operations or scenarios involving repeated trajectories, where loop-closure mechanisms can be exploited to maintain consistency. The approach presented in this work instead leverages georeferenced prior information, enabling absolute positioning without the need to build a map during operation. This characteristic allows navigation over previously unvisited areas, provided that prior intelligence data is available, and makes the solution compatible with high-altitude and wide-area mission profiles.

Finally, multiple algorithmic approaches are considered for the visual modules, including feature-based and learning-based methods. This design choice is enabled by the modular architecture of the ALTERNATIVE Core and allows systematic evaluation of trade-offs between robustness, accuracy, and computational cost. Such flexibility is critical for transitioning from experimental validation to deployable solutions, where performance must be maintained under diverse and challenging operational conditions.

4 Testing Methodology

The evaluation methodology adopted in this work is structured to ensure a controlled and reproducible assessment of the proposed navigation framework. Rather than analysing isolated algorithmic performance, the objective is to evaluate the behaviour of the complete PNT architecture under realistic operational conditions.

In this study, the classical GNSS + IMU configuration is used as a well-established navigation reference against which the visual-aided configurations are compared. The experiments are designed to assess the behaviour of the different sensor combinations over predefined trajectories and for a fixed UAS dynamic model, ensuring that all configurations are evaluated under identical conditions.

Hardware-in-the-Loop environment is used as the experimental setup, as previously described in Section 3, which allows runtime execution of the navigation chain. This approach enables not only the measurement of positioning accuracy, but also the analysis of estimator stability, drift behaviour and robustness under GNSS-degraded scenarios.

Performance evaluation is based on complementary metrics, including positional RMSE and drift rate, allowing both accumulated error and temporal error growth to be characterised. This dual-metric analysis provides insight into the relative contribution of visual measurements and facilitates identification of dominant error sources, such as sporadic outliers affecting the estimation process.

The following subsections describe the different experimental scenarios defined according to this evaluation framework.

Except where otherwise noted, content of this paper is licensed under a Creative Commons Attribution 4.0 International License.

The reproduction and distribution with attribution of the entire paper or of individual pages, in electronic or printed form, including any material under non-CC-BY 4.0 licenses is hereby granted by the authors and respective copyright owners.

4.1 Experiments objectives and hypothesis

The experiments carried out in this work aim to replicate representative real-world operational scenarios in order to verify the behaviour of the proposed navigation system under different conditions. The objective is twofold. On the one hand, the performance of the developed algorithms is assessed. On the other hand, the robustness of the overall system is evaluated when subjected to a variety of operational situations.

The tested scenarios include both nominal operating conditions and deliberately induced off-nominal situations, such as simulated functional degradations and hardware failures. These experiments enable the evaluation of the Fault Detection, Isolation and Recovery (FDIR) mechanisms implemented in the software, verifying that the system can preserve a consistent and reliable navigation solution even under adverse conditions.

These validation activities are particularly relevant for navigation systems intended for deployment in real unmanned aircraft systems, as considered in this work. Although the current development corresponds to a moderate Technology Readiness Level (TRL), the experimental framework and validation strategy have been designed to support future iterations of the system, facilitating its evolution towards higher maturity levels, potentially reaching TRL values between 7 and 9.

In the current development, the simulated sensors include an IMU, a GNSS receiver and a camera. Each sensor model receives as input a predefined trajectory generated over different operational areas. Based on this trajectory, the sensor simulators reproduce the expected functional behaviour of their real counterparts under the corresponding dynamic and environmental conditions. A key aspect of the simulation framework is time synchronisation. All simulated sensors are synchronised through an external PPS reference.

The trajectory simulator includes operational constraints consistent with the expected flight envelope of the target UAS. These constraints currently limit the maximum translational velocity, angular rates and operational altitude. Such bounds ensure dynamic consistency between the simulated platform and the intended deployment conditions. However, this configuration can be adapted in order to emulate different platforms, allowing the system to be evaluated for deployment in other UAS types with distinct dynamic characteristics.

Regarding the camera model, all experiments were conducted under the assumption of a fixed camera configuration. A ”gimbal” type of camera was locked in a downward-looking (zenithal) orientation throughout the missions, eliminating variability associated with camera dynamics, pointing errors, or active stabilisation behaviour. Additionally, all tests were carried out under ideal visual conditions. The simulated environment assumed a planar world model, clear weather with uniform illumination (e.g., a sunny day), absence of atmospheric effects, and no platform-induced disturbances such as vibrations or abrupt attitude changes.

4.2 Dataset definition and analysis

The camera simulation is currently based on satellite imagery extracted from a georeferenced database. Images from different years are used in order to introduce temporal variability in the visual appearance of the terrain. This approach allows the evaluation of the visual navigation algorithms under more realistic conditions, accounting for seasonal changes, urban evolution and landscape modifications over time.

At this stage of development, the simulated images are limited to RGB data. Multispectral or infrared modalities are not yet considered, although the simulation framework has been designed to accommodate additional spectral bands in future iterations.

Although the simulator is capable of generating trajectories over any geographic location, the visual database is presently restricted to Spanish territory. This limitation is associated with the availability

Except where otherwise noted, content of this paper is licensed under a Creative Commons Attribution 4.0 International License.

The reproduction and distribution with attribution of the entire paper or of individual pages, in electronic or printed form, including any material under non-CC-BY 4.0 licenses is hereby granted by the authors and respective copyright owners.

and preprocessing of high-resolution satellite imagery. The geographic coverage will be progressively extended in future developments in order to evaluate the system under a broader range of terrain types, climatic conditions and visual characteristics.

4.3 Experimental campaign definition

A set of 26 operational vignetes was conducted to evaluate the system from different perspectives, covering different sensor configurations, heights and trajectories. A subset of the tests focused on assessing the system behaviour under simulated sensor failures and analysing the response of the PNT solution to such events. These activities contribute to verifying the robustness of the architecture and support the safe deployment of the PNT system in the aircraft. Although these tests are needed, they are primarily part of the project Verification and Validation process and are therefore not detailed in this article.

Three navigation configurations have been defined for the present functional assessment:

Configuration 1: The first configuration consists of a tightly coupled GNSS/IMU fusion scheme, which serves as the reference configuration for performance benchmarking. In this mode, absolute position and velocity updates from GNSS measurements are fused with inertial mechanisation to bound drift and provide a nominal navigation solution representative of standard operation in GNSS-available conditions. Using this configuration as the baseline allows a direct and unambiguous comparison between the predicted outputs of visual algorithms and the nominal trajectory, thereby isolating algorithmic performance from external factors.

Configuration 2: The second configuration extends the previous architecture by incorporating visual inputs into the estimation framework. In this multi-sensor fusion mode, visual measurements are integrated alongside GNSS and IMU data within the state estimator, improving observability and robustness, particularly in scenarios with degraded satellite geometry or intermittent signal availability. This mode allows quantifying the incremental contribution of visual measurements to the overall state estimation performance, in terms of accuracy, consistency, and drift mitigation, as well as assessing their impact on estimator stability and convergence behaviour under nominal and mildly degraded conditions.

Configuration 3: The third configuration corresponds to a GNSS-denied operational mode. In this case, the navigation solution is propagated through inertial mechanisation using the IMU, while drift is mitigated through corrections derived from visual measurements. This configuration is intended to assess estimator stability, error growth behaviour and overall performance in the absence of external GNSS updates.

For performance assessment, these three configurations are compared with the ground truth generated by the simulator. This reference was chosen because it represents the exact intended flight plan, free from sensor noise, environmental disturbances, or modelling uncertainties.

The experimental campaigns were conducted using a set of predefined trajectories. All configurations were evaluated over the same trajectory profiles in order to ensure a consistent and fair performance comparison. This approach guarantees that any observed differences in the navigation solution are attributable to the configuration itself rather than to variations in the flight path.

The selected trajectories were defined at three different operational altitudes, namely 1000 m, 1500 m and 3000 m. In addition, different geometric patterns were considered, including a linear path, a circular trajectory and a figure-eight manoeuvre. These trajectory shapes were chosen to introduce variations in dynamics, heading changes and curvature, allowing evaluation of the estimator behaviour under diverse motion conditions.

The total trajectory lengths ranged approximately between 5 000 m and 6 500 m, corresponding to the longest simulated cases. Although minor variations in path length exist, these differences do not compromise the comparability of the results, since all configurations were evaluated over the same

Except where otherwise noted, content of this paper is licensed under a Creative Commons Attribution 4.0 International License.

The reproduction and distribution with attribution of the entire paper or of individual pages, in electronic or printed form, including any material under non-CC-BY 4.0 licenses is hereby granted by the authors and respective copyright owners.

trajectory profile within each individual experiment. Furthermore, the selected trajectory lengths are representative of medium-range UAS operations and are sufficient to capture both transient estimator behaviour and long-term error accumulation effects.

All simulations were conducted over Spanish territory, covering different types of terrain. The selected areas include regions with dense vegetation as well as more arid or sparsely textured zones.

4.4 Metrics

To correctly evaluate the behaviour of the system two different metrics were selected for the study.

The primary metric used to evaluate navigation performance is the positional RMSE. This metric quantifies the average deviation of the estimated position with respect to the reference trajectory over the entire experiment. The RMSE provides a global and statistically meaningful measure of accuracy, penalising large deviations more strongly than small ones. For this reason, it serves as a baseline indicator when comparing the performance of the different navigation configurations.

However, while the RMSE captures the overall positioning accuracy, it does not provide information about the temporal evolution of the error. In particular, it does not characterise how the estimation error grows in time during periods of degraded aiding or reduced observability. For this reason, an additional metric based on drift per unit time is introduced. This metric evaluates the rate at which the positional error increases, typically expressed in metres per second, and is especially relevant in scenarios with limited or intermittent GNSS availability.

The inclusion of the drift metric complements the RMSE by providing insight into the stability and robustness of the estimator. While the RMSE reflects accumulated accuracy over the trajectory, the drift rate characterises the dynamic behaviour of the navigation solution and its sensitivity to error propagation.

5 Results and Discussion

Tab. 1 shows the overall results of the positioning error for the three sensor configurations test. All three configurations contain the IMU, as explained in Section 4.3

Table 1 Positional RMSE per Sensors Configuration

Sensors Configuration	RMSE [m]
Configuration 1: Nominal GNSS + IMU	15.11
Configuration 2: GNSS + IMU and CAMERA	16.30
Configuration 3: IMU + CAMERA	32.09

The obtained results indicate that the visual-aided navigation configuration does not reach the absolute positioning performance of the traditional GNSS/IMU architecture. This outcome was anticipated, given that GNSS provides highly accurate absolute positioning measurements and constitutes a mature and well-established technology. In contrast, visual navigation relies on indirect environmental features whose quality depends on texture richness, illumination conditions and scene geometry.

A direct comparison with other state-of-the-art visual navigation solutions is not straightforward. Performance metrics reported in the literature are often obtained under different experimental conditions, including variations in UAS speed, trajectory length, altitude, sensor characteristics and terrain type. Since these factors strongly influence the behaviour of visual navigation algorithms, a fair comparison would require harmonised testing conditions.

Despite these limitations, the results demonstrate that the visual configuration maintains stable and consistent performance over trajectories exceeding 5 000 m, which corresponds to the minimum path

Except where otherwise noted, content of this paper is licensed under a Creative Commons Attribution 4.0 International License.

The reproduction and distribution with attribution of the entire paper or of individual pages, in electronic or printed form, including any material under non-CC-BY 4.0 licenses is hereby granted by the authors and respective copyright owners.

length evaluated in this work, as described in Section 4.3. Even for trajectories involving significant curvature variations, such as circular and figure-eight patterns, the visual-aided solution remains within the same order of magnitude as the classical GNSS/IMU baseline.

An additional aspect of interest is the influence of operational altitude on navigation performance. Changes in height affect image resolution, ground sampling distance and feature density, all of which directly impact visual estimation accuracy. This analysis is presented in Fig. **??** and summarised in Table 2.

Table 2 Height Effect on the Positional RMSE

Sensors configuration	1000m altitude [m]	1500m altitude [m]	3000m altitude [m]
Configuration 1: Nominal GNSS + IMU	14.08	15.11	17.67
Configuration 2: GNSS + IMU and CAMERA	13.37	18.09	16.35
Configuration 3: IMU + CAMERA	23.23	28.43	44.39

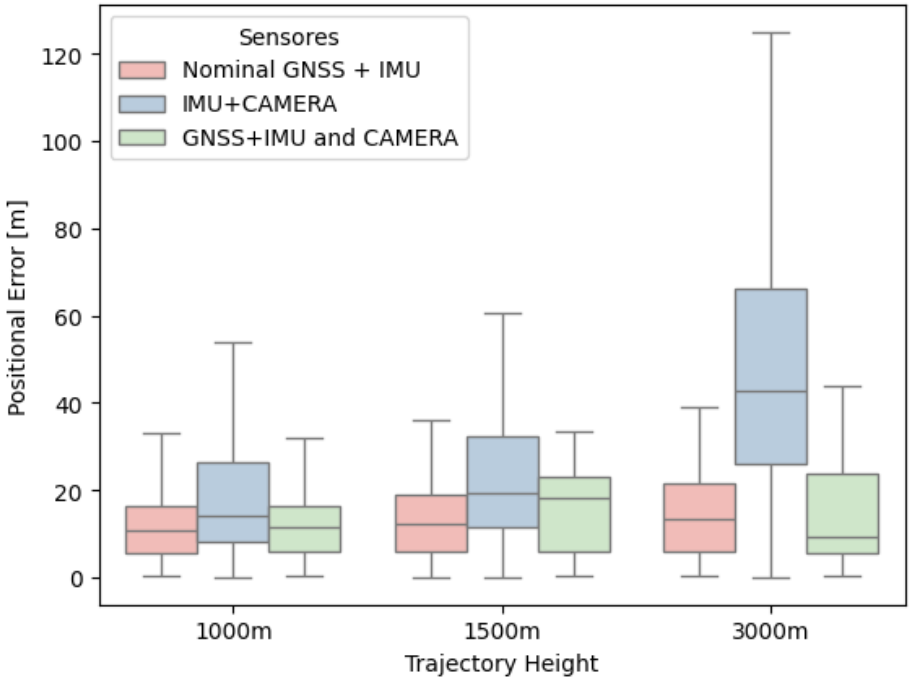

Fig. 3 Positional Error Distribution per Height

The results indicate that visual navigation performance degrades as operational altitude increases. At higher flight levels, the effective ground sampling distance becomes larger, reducing the spatial resolution of the observed terrain. As a consequence, the number of distinctive and repeatable features available for matching decreases. In addition, higher altitudes tend to reduce texture richness and increase ambiguity in feature association, leading to a greater probability of mismatches and outliers. This behaviour is illustrated in Fig. **??**, where the dispersion of the positional error increases for the configurations incorporating visual navigation at higher altitudes.

For analysing all the obtained results is also interesting to study the drift evaluation for sensor configuration as shown in Table 3.

Except where otherwise noted, content of this paper is licensed under a Creative Commons Attribution 4.0 International License.

The reproduction and distribution with attribution of the entire paper or of individual pages, in electronic or printed form, including any material under non-CC-BY 4.0 licenses is hereby granted by the authors and respective copyright owners.

Table 3 Drift evaluation per sensor configuration

Sensors configuration	Drift over time [m/s]	R^2
Configuration 1: Nominal GNSS + IMU	-0.009	0.7%
Configuration 2: GNSS + IMU and CAMERA	-0.014	1.2%
Configuration 3: IMU + CAMERA	-0.067	0.3%

It can be observed that accumulated drift is not the sole contributor to the error values reported in Table 1. The relatively low drift rates, together with the limited linear correlation coefficients, indicate that the positioning error does not grow purely in a linear manner over time. Instead, a significant portion of the total error is associated with sporadic deviations, suggesting the presence of outliers that introduce abrupt perturbations in the navigation solution.

These sporadic deviations are especially significant in the visual-aided configurations, where measurement reliability strongly depends on feature quality and scene texture. In regions characterised by low texture richness or limited visual contrast, the probability of incorrect feature associations increases. Such mismatches introduce transient but potentially large estimation errors that manifest as outliers in the navigation solution. Consequently, overall navigation performance could be enhanced by integrating more robust statistical consistency mechanisms within the EKF framework.

6 Conclusion

This work has presented and experimentally assessed a visual-aided navigation architecture for small UAS operating in degraded or denied GNSS environments. The relevance of the proposed approach lies in its ability to extend navigation robustness beyond the limits of conventional GNSS/IMU solutions, while avoiding the operational constraints of many state-of-the-art vision-based methods that depend on online map generation or repeated trajectories. By combining inertial sensing, GNSS, visual odometry, and map correlation within a unified EKF framework, the architecture enables first-pass navigation capabilities over previously unvisited areas, provided that georeferenced prior information is available.

Compared with alternative methodologies, the proposed solution does not aim to outperform nominal GNSS in absolute positioning under favourable signal conditions, which remains the reference in terms of mature and highly accurate navigation performance. Instead, its contribution is to provide a resilient complementary navigation capability when GNSS becomes unreliable or unavailable. In this respect, the results show that the visual-aided solution remains stable over representative UAS trajectories and preserves bounded performance even in GNSS-denied conditions, whereas standalone inertial navigation would be expected to exhibit unbounded drift growth. Moreover, in contrast to SLAM-based approaches, the proposed architecture does not require online map construction, making it better suited to wide-area, higher-altitude, and first-deployment mission profiles.

The results also indicate that the current performance limitation is not dominated by progressive drift alone, but by sporadic outliers associated with degraded visual conditions, feature ambiguity, and reduced scene texture. This finding is important because it shifts the focus of future improvement from simply refining low-level odometry accuracy towards strengthening the statistical robustness of the fusion process. In particular, the main path forward is the development of more robust measurement validation, outlier rejection, and consistency-monitoring mechanisms within the EKF framework.

The next stage of this work will therefore focus on improving robustness to visual outliers, extending the validation campaign to more diverse terrains and sensing conditions, and progressing from the present Hardware-in-the-Loop environment to full flight-test evaluation on the target aerial platform. These

Except where otherwise noted, content of this paper is licensed under a Creative Commons Attribution 4.0 International License.

The reproduction and distribution with attribution of the entire paper or of individual pages, in electronic or printed form, including any material under non-CC-BY 4.0 licenses is hereby granted by the authors and respective copyright owners.

steps are required to consolidate the proposed architecture as a practical resilient PNT solution for future operational UAS missions.

Acknowledgements

The authors would like to acknowledge the valuable contributions of the visual navigation team, whose work was instrumental in the development and validation of the visual-aided components of this research: Mikel Loinaz Anton, Enrique Lozoya Lidón, Luís Navarro García, Lluís Arrué Vicedo, Mario González-Román Blanco, Alejandro Cortijo Benito, Jorge Varadé Varea, and Víctor Herranz Sánchez.

The authors also express their sincere gratitude to the INDRA team for their support during the experimental campaigns with the aerial platform environment: Sergio Vigorra Treviño, José María Calero Barón, and Álvaro García Domínguez.

This work has been supported by the European Defence Agency (EDA), whose funding and strategic guidance have been essential for advancing research on resilient navigation solutions in GNSS-contested environments.

Declaration of Use of Artificial Intelligence

During the preparation of this paper, the authors used ChatGPT to assist with improving the translation of the manuscript. All translations produced with its help was carefully reviewed and edited by the authors, who take full responsibility for the final content of the published article.

References

[1] P. D. Groves. *Principles of GNSS, Inertial, and Multisensor Integrated Navigation Systems*. Artech House, 2013.

[2] Arman Asgharpoor Golroudbari and Mohammad Hossein Sabour. Generalizable end-to-end deep learning frameworks for real-time attitude estimation using 6dof inertial measurement units. *Measurement*, 217:113105, 2023.

[3] Jieqiong Wang and Wenguang Jin. Inertial measurement unit calibration method based on neural network. In *2023 16th International Congress on Image and Signal Processing, BioMedical Engineering and Informatics (CISP-BMEI)*, pages 1–6. IEEE, 2023.

[4] A Kassner, L Diekmann, C Künzler, J Petring, N Droese, F Dencker, H Heine, S Abend, M Gersemann, EM Rasel, et al. Miniaturized quantum systems for inertial measurement units. In *2023 DGON Inertial Sensors and Systems (ISS)*, pages 1–20. IEEE, 2023.

[5] M Gersemann, A Rajagopalan, M Abidi, P Barbey, A Sabu, X Chen, NB Weddig, B Tennstedt, J Petring, N Droese, et al. Developments for quantum inertial navigation systems employing bose–einstein condensates. *Applied Physics Reviews*, 12(3), 2025.

[6] Narges Kafaei and Ali Motazedifard. A short introduction to basic principles of quantum navigation based-on rb cold atom interferometry. *arXiv preprint arXiv:2405.14910*, 2024.

[7] Benjamin Tennstedt, Ashwin Rajagopalan, Nicolai B Weddig, Sven Abend, Steffen Schön, and Ernst M Rasel. Atom strapdown: Toward integrated quantum inertial navigation systems. *NAVIGATION: Journal of the Institute of Navigation*, 70(4), 2023.

[8] Aaron Canciani and John Raquet. Airborne magnetic anomaly navigation. *IEEE Transactions on aerospace and electronic systems*, 53(1):67–80, 2017.

Except where otherwise noted, content of this paper is licensed under a Creative Commons Attribution 4.0 International License.

The reproduction and distribution with attribution of the entire paper or of individual pages, in electronic or printed form, including any material under non-CC-BY 4.0 licenses is hereby granted by the authors and respective copyright owners.

[9] Taylor N Lee and Aaron J Canciani. Aerial simultaneous localization and mapping using earth's magnetic anomaly field. In *Proceedings of the 2019 International Technical Meeting of the Institute of Navigation*, pages 471–485, 2019.

[10] Donna M Kocak, Benjamin Thayer, Haley Stumvoll, Jim Drakes, and Chris Hessenius. Quantum magnetometry for enhanced sensing in autonomous underwater vehicles. In *OCEANS 2024-Halifax*, pages 1–7. IEEE, 2024.

[11] Ziyun Yu, Yunbin Zhu, Wenzhe Zhang, Ke Jing, Shuo Wang, Chuanxu Chen, Yijin Xie, Xing Rong, and Jiangfeng Du. Experimental demonstration of a diamond quantum vector magnetometer for deep-sea applications. *National Science Review*, 12(4):nwae478, 2025.

[12] Xuezhi Wang, Wenchao Li, Bill Moran, Brant C Gibson, Liam T Hall, DA Simpson, Allison N Kealy, and Andrew D Greentree. Quantum diamond magnetometry for navigation in gnss denied environments. In *IAG International Symposium on Reference Frames for Applications in Geosciences*, pages 87–92. Springer Nature Switzerland Cham, 2022.

[13] C. Campos, R. Elvira, J. J. Gómez Rodríguez, J. M. Montiel, and J. D. Tardós. Orb-slam3: An accurate open-source library for visual, visual–inertial, and multi-map slam. *IEEE Transactions on Robotics*, 2021. doi: 10.1109/TRO.2021.3075644.

[14] Martin Rebert. *Two views camera motion in the presence of planar degeneracy*. PhD thesis, Université de Haute Alsace-Mulhouse, 2020.

[15] Jouko Kinnari, Francesco Verdoja, and Ville Kyrki. Season-invariant gnss-denied visual localization for uavs. *IEEE Robotics and Automation Letters*, 7(4):10232–10239, 2022.

[16] Obin Kwon, Jeongho Park, and Songhwai Oh. Renderable neural radiance map for visual navigation. In *Proceedings of the IEEE/CVF Conference on Computer Vision and Pattern Recognition*, pages 9099–9108, 2023.

[17] Jiuhong Xiao, Ning Zhang, Daniel Tortei, and Giuseppe Loianno. Sthn: Deep homography estimation for uav thermal geo-localization with satellite imagery. *IEEE Robotics and Automation Letters*, 2024.

[18] Ganchao Liu, Chao Li, Sihang Zhang, and Yuan Yuan. Vl-mfl: Uav visual localization based on multisource image feature learning. *IEEE Transactions on Geoscience and Remote Sensing*, 62:1–12, 2024.

[19] Weibo Xu, Dongfang Yang, Jieyu Liu, Yongfei Li, and Maoan Zhou. A visual navigation algorithm for uav based on visual-geography optimization. *Drones*, 8(7):313, 2024.

[20] Jorge F. García-Samartín, Christyan Cruz Ulloa, Jaime del Cerro, and Antonio Barrientos. Active Robotic Search for Victims using Ensemble Deep Learning Techniques. *Machine Learning: Science and Technology*, 5, 2024. doi: 10.1088/2632-2153/ad33df.

[21] VectorNav Technologies. Vn-300 dual GNSS / IMU datasheet. Technical report, VectorNav Technologies LLC, Dallas, Texas, USA. Dual-antenna GNSS-aided MEMS IMU providing real-time attitude and position estimation for UAV applications. https://www.navtechgps.com/wp-content/uploads/VN-300_DS.pdf.

[22] Honeywell Aerospace. Hg9900 inertial navigation system datasheet. Technical report, Honeywell International Inc., Phoenix, Arizona, USA, 2011. Datasheet describing the HG9900 inertial/GNSS navigation system for aircraft and UAVs. https://lkdaerospace.com/wp-content/uploads/hg9900imu.pdf.

[23] a Safran Company Orolia. VersaPNT integrated PNT system technical datasheet. Technical report, Orolia Defense and Security, Rochester, New York, USA. High-performance positioning, navigation and timing unit integrating GNSS, IMU and an atomic clock for resilient PNT. https://image.discover.safranfs.com/lib/fe30 11747364047875127 5/m/1/9a484f47-af5c-4c25-a495-aa0ce479757d.pdf.

Except where otherwise noted, content of this paper is licensed under a Creative Commons Attribution 4.0 International License.

The reproduction and distribution with attribution of the entire paper or of individual pages, in electronic or printed form, including any material under non-CC-BY 4.0 licenses is hereby granted by the authors and respective copyright owners.

[24] Northrop Grumman Corporation. Ln-200 fiber optic gyro IMU. Technical report, Northrop Grumman Navigation Systems Division, Woodland Hills, California, USA. Tactical-grade FOG IMU used in aerospace, land and naval navigation systems. https://cdn.northropgrumman.com/-/media/Project/Northrop-Grumman/ngc/what-we-do/air/ln-200-fog-family-advanced-airborne/LN-200-FOG-Family-datasheet.pdf?rev=14284f2e4e41401f8d056533672fb76d.

[25] Exail (formerly iXblue). UMIX-40-5du IMU datasheet. Technical report, Exail, Saint-Germain-en-Laye, France. Fiber-Optic Gyroscope IMU for UAV and robotic navigation applications. https://www.exail.com/media-file/98/exail-datasheet-umix-40-5du-imu.pdf.

[26] Sensonor AS. Stim318 tactical grade IMU datasheet. Technical report, Sensonor AS, Horten, Norway. Tactical-grade MEMS IMU with low noise, low bias instability and high reliability for UAV and land navigation. https://safran-navigation-timing.com/document/stim318-datasheets/.

[27] J. Zhang and S. Singh. Loam: Lidar odometry and mapping in real-time. In *Robotics: Science and Systems*, 2014.

[28] T. Qin, P. Li, and S. Shen. Vins-mono: A robust and versatile monocular visual-inertial state estimator. *IEEE Transactions on Robotics*, 2018.

[29] Inertial Labs. Vision-aided inertial navigation system (VINS) datasheet rev. 1.9. Technical report, Inertial Labs, a VIAVI Solutions Company, Ashburn, Virginia, USA, 2025. Datasheet describing the VINS system for UAVs and ground platforms operating in GNSS-challenged environments. https://www.scribd.com/document/918294516/VINS-Datasheet-rev1-9-April9-2025.

[30] Bavovna AI. Ai navigation kit for UAVs: Hybrid INS solution for GPS-denied environments. Technical report, Bavovna AI, Austin, TX, USA / Kyiv, Ukraine, 2024. Datasheet describing the Bavovna AI hybrid INS and machine-learning-based navigation kit for UAVs. https://bavovna.ai/ai-navigation-kit/.

[31] T. Shan and B. Englot. Lio-sam: Tightly-coupled lidar inertial odometry via smoothing and mapping. In *IEEE/RSJ International Conference on Intelligent Robots and Systems (IROS)*, 2020.

[32] M. Bloesch, S. Omari, M. Hutter, and R. Siegwart. Robust visual inertial odometry using a direct ekf-based approach. In *IEEE/RSJ International Conference on Intelligent Robots and Systems (IROS)*, 2015.

[33] HKUST Aerial Robotics Group. A-loam: Advanced lidar odometry and mapping. https://github.com/HKUST-Aerial-Robotics/A-LOAM. Accessed: 2025-10-30.

[34] Q. Gong, D. Virette, A. Martin, and J. Salden. Magnetometer-aided gyroscope and accelerometer calibration: Magneto-inertial sensor alignment without external reference. *IEEE Sensors Journal*, 17(2):498–508, 2017.

[35] A. Solin, S. Särkkä, and J. Suomela. Terrain navigation by exploiting magnetic anomaly maps. *IEEE Transactions on Robotics*, 32(3):625–636, 2016.

[36] R. E. Kalman. A new approach to linear filtering and prediction problems. *Journal of Basic Engineering*, pages 35–45, 1960.

[37] Y. Bar-Shalom, X. R. Li, and T. Kirubarajan. *Estimation with Applications to Tracking and Navigation*. Wiley, 2001.

Except where otherwise noted, content of this paper is licensed under a Creative Commons Attribution 4.0 International License.

The reproduction and distribution with attribution of the entire paper or of individual pages, in electronic or printed form, including any material under non-CC-BY 4.0 licenses is hereby granted by the authors and respective copyright owners.